Generalised Langevin model in correspondence with a chosen standard scalar-flux second-moment closure

B. Naud – B. Merci – D. Roekaerts

In: Flow Turbulence and Combustion, Volume 85, Issue 3-4, pp. 363-382, 2010

Editorial Manager(tm) for Flow, Turbulence and Combustion
Manuscript Draft

Manuscript Number: APPL2804R1

Title: Generalised Langevin model in correspondence with a chosen standard scalar-flux second-moment closure

Article Type: SI: Pope

Keywords: Generalised Langevin Model (GLM); Differential scalar-flux model; Diffusion coefficient C_0; Mixing model dependence on velocity.

Corresponding Author: Dr Bertrand Naud, PhD

Corresponding Author's Institution: CIEMAT

First Author: Bertrand Naud, PhD

Order of Authors: Bertrand Naud, PhD; Bart Merci, PhD; Dirk Roekaerts, PhD

Manuscript Region of Origin: SPAIN

Abstract: In the context of transported joint velocity-scalar probability density function methods, the correspondence between Generalised Langevin Models (GLM) for Lagrangian particle velocity evolution and Eulerian Reynolds-stress turbulence models has been established in the 1990's by S.B. Pope. It was shown that the GLM representation of a given Reynolds stress model is not unique. It was also shown that a given GLM together with a given mixing model for particle composition evolution implies a differential scalar-flux model. In this paper, we study how extra constraints can be applied on the choice of the GLM coefficients in order to imply a chosen scalar-flux model. This correspondence between GLM-implied and standard scalar-flux models is based on the linear relaxation term and on the mean velocity gradient contributions in the rapid term. In general, GLM-implied models possibly involve more terms (including anisotropy effects in the scalar-flux decay rate and some high-order terms in the rapid-pressure-scrambling term). The proposed form of the GLM supposes a non-constant value for the diffusion coefficient C0, originally identified as a Kolmogorov constant. Here, the value of C0 is determined in order to yield the Monin model for linear relaxation of the scalar-flux, and the constant in the rapid-pressure contribution is related to the choice of the parameter $\beta*$ in the GLM. We finally show how GLM-implied scalar-flux models are in general dependent on the choice of the mixing model and how the proposed GLM can reduce this dependency. These developments are illustrated by results obtained from calculations of the Sydney bluff-body stabilised flame HM1.

Response to Reviewers: First of all, we would like to thank the reviewers for their comments which helped to improve the paper.

#1
We included all the suggestions of Reviewer #1. About remark 5: we used the more general formalism introduced by Wouters [REF. 4] that allows to deal with variable density flows, and with Reynolds-stress models that include cubic terms (we added a remark in the text after Equation (27) at the beginning of Section 4.1).

#2

The remarks of Reviewer #2 allowed us to distinguish more clearly in the text two aspects: 1. setting the C_0 value depending on the Monin linear relaxation term and 2. removing the effect of the mixing model as much as possible. This lead to some modifications of the text. The modification of $\beta*$ in order to be in agreement with Launder's model for the rapid-pressure-scrambling term is indeed pragmatic. We added some clarifications on this aspect on page 12 in the paragraph "Rapid-pressure-scrambling term".
About the "philosophical questions" raised by the reviewer, here are some remarks on the modification of C_0 in order to lead the Monin linear return to isotropy (the main contribution of this paper). As mentioned by the reviewer "the scalar field is dynamically passive". With Taylor's hypothesis, we see the relation between the Monin constant and the GLM coefficient C_0. As discussed in the paper, there is no reason why C_0 should be a constant, and we know that the value 2.1 is probably too low (note that S.B. Pope proposed the model IPMb where C_0 is not a constant).

#3
In order to deal with the three points proposed by Reviewer #3, we made the following changes:
1. we added a new paragraph in section 4.2, entitled: "Perfect match between GLM-implied model and standard model?".
2. we modified the text everywhere where we were talking about "localness in velocity space of the mixing model", rather talking about "dependence of the mixing model on velocity". We added a new paragraph in section 3.2, entitled: "Mixing model dependence on velocity".
3. we specified that we considered a single conserved scalar case in the two statements mentioned by the reviewer.

Flow, Turbulence and Combustion manuscript No.
(will be inserted by the editor)

Generalised Langevin model in correspondence with a chosen standard scalar-flux second-moment closure

Bertrand Naud · Bart Merci · Dirk Roekaerts

Received: date / Accepted: date

Abstract In the context of transported joint velocity-scalar probability density function methods, the correspondence between Generalised Langevin Models (GLM) for Lagrangian particle velocity evolution and Eulerian Reynolds-stress turbulence models has been established in the 1990's by S.B. Pope. It was shown that the GLM representation of a given Reynolds stress model is not unique. It was also shown that a given GLM together with a given mixing model for particle composition evolution implies a differential scalar-flux model. In this paper, we study how extra constraints can be applied on the choice of the GLM coefficients in order to imply a chosen scalar-flux model. This correspondence between GLM-implied and standard scalar-flux models is based on the linear relaxation term and on the mean velocity gradient contributions in the rapid term. In general, GLM-implied models possibly involve more terms (including anisotropy effects in the scalar-flux decay rate and some high-order terms in the rapid-pressure-scrambling term). The proposed form of the GLM supposes a non-constant value for the diffusion coefficient C_0, originally identified as a Kolmogorov constant. Here, the value of C_0 is determined in order to yield the Monin model for linear relaxation of the scalar-flux, and the constant in the rapid-pressure contribution is related to the choice of the parameter β^* in the GLM. We finally show how GLM-implied scalar-flux models are in general dependent on the choice of the mixing model and how the proposed GLM can reduce this dependency. These developments are illustrated by results obtained from calculations of the Sydney bluff-body stabilised flame HM1.

Keywords Generalised Langevin Model (GLM) · Differential scalar-flux model · Diffusion coefficient C_0 · Mixing model dependence on velocity

B. Naud
Modeling and Numerical Simulation Group, Energy Department, Ciemat,
Avda. Complutense 22, 28040 Madrid, Spain
E-mail: bertrand.naud@ciemat.es

B. Merci
Department of Flow, Heat and Combustion Mechanics, Ghent University, Ghent, Belgium

D. Roekaerts
Department of Multi-Scale Physics, Delft University of Technology, Delft, The Netherlands

1 Introduction

In the framework of RANS modelling of turbulent non-premixed flames, transported probability density function (PDF) methods introduced by S.B. Pope [1] have proven to be powerful methods when finite-rate chemistry needs to be considered. Crucial aspects of non-linear interaction between turbulent fluctuations and finite-rate chemistry can indeed be accounted for, such as auto-ignition, local extinction and re-ignition, or incomplete combustion.

In the context of one-point statistical modelling of turbulent flows (reacting or non-reacting), from the modelling assumptions made at the level of the one-point joint velocity-scalar PDF (i.e. from the chosen Langevin model and from the chosen mixing model), second-moment closure models can be retrieved [2]. This is a useful way to derive consistent and realisable second-moment closures [3]. The other way around, the Langevin model can be specified such that it corresponds to a given Reynolds-stress model [2,4]. Still, the choice for a Langevin model corresponding to a given Reynolds-stress model is not unique.

In this paper, additional constraints are applied to the Generalised Langevin Model (GLM) coefficients such that a chosen scalar-flux model is implied (still in correspondence with a chosen Reynolds-stress model). We first present the general modelling framework for transported joint velocity-scalar PDF (JVSPDF) methods. We then comment on the models used at the PDF level and the implied second-moment closures for Reynolds stresses and scalar fluxes. We stress the fact that mixing models which are independent of velocity (like the most widely used mixing models) imply an extra contribution in the model for the pressure-scrambling term. The next section focuses on the main purpose of this paper: the construction of a GLM in correspondence with a given differential scalar-flux model. Following [2], a formulation with constant diffusion coefficient C_0 is first recalled, and a formulation consistent with a chosen standard scalar-flux model is then proposed. The latter, which does not use a constant value for the coefficient C_0, can reduce the dependency on the mixing model. Finally, considering the Sydney bluff-body stabilised flame HM1 [5,6], results obtained with different models are presented in the light of the modelling issues previously discussed.

2 Joint velocity-scalar PDF

2.1 Statistical description at one point

The statistical description of the flow is made in terms of the joint one-point PDF $f_{\boldsymbol{\Phi}}$ such that $f_{\boldsymbol{\Phi}}(\boldsymbol{\Psi};\boldsymbol{x},t)\,.\mathrm{d}\boldsymbol{\Psi}$ is the probability that $\boldsymbol{\Phi}$ is in the interval $[\boldsymbol{\Psi},\boldsymbol{\Psi}+\mathrm{d}\boldsymbol{\Psi}[$ at point $(\boldsymbol{x},t)$. We consider the joint velocity-composition PDF such that $\boldsymbol{\Phi}=(\boldsymbol{U},\boldsymbol{\phi})$, with $\boldsymbol{U}$ the velocity vector and $\boldsymbol{\phi}$ the composition vector. The joint PDF is defined as [1,7]: $f_{\boldsymbol{\Phi}}(\boldsymbol{\Psi};\boldsymbol{x},t)=\langle\delta[\boldsymbol{\Phi}(\boldsymbol{x},t)-\boldsymbol{\Psi}]\rangle$, where $\delta[\,]$ is the Dirac delta function and where the brackets $\langle\,\rangle$ refer to the expected value [7]. Using the conditional expected value [1], $\langle Q(\boldsymbol{x},t)|\,\boldsymbol{\Psi}\rangle f_{\boldsymbol{\Phi}}(\boldsymbol{\Psi};\boldsymbol{x},t)=\langle Q(\boldsymbol{x},t)\,.\delta[\boldsymbol{\Phi}(\boldsymbol{x},t)-\boldsymbol{\Psi}]\rangle$, mean values (or expected values) $\overline{Q}$ and fluctuations q' are defined as:

$$\overline{Q}=\langle Q(\boldsymbol{x},t)\rangle=\int_{[\boldsymbol{\Psi}]}\langle Q(\boldsymbol{x},t)|\,\boldsymbol{\Psi}\rangle f_{\boldsymbol{\Phi}}(\boldsymbol{\Psi};\boldsymbol{x},t)\,.\mathrm{d}\boldsymbol{\Psi}\qquad\text{and}\qquad q'=Q-\overline{Q}. \tag{1}$$

For variable density flows, it is useful to consider the joint mass density function (MDF) $\mathcal{F}_\Phi(\boldsymbol{\Psi}) = \rho(\boldsymbol{\Psi})\, f_\Phi(\boldsymbol{\Psi})$. Density weighted averages (Favre averages) can be considered:

$$\widetilde{Q} = \frac{\langle \rho(\boldsymbol{x},t)\, Q(\boldsymbol{x},t)\rangle}{\langle \rho(\boldsymbol{x},t)\rangle} = \frac{\int_{[\boldsymbol{\Psi}]} \langle Q(\boldsymbol{x},t)|\, \boldsymbol{\Psi}\rangle \mathcal{F}_\Phi(\boldsymbol{\Psi};\boldsymbol{x},t)\, .\mathrm{d}\boldsymbol{\Psi}}{\int_{[\boldsymbol{\Psi}]} \mathcal{F}_\Phi(\boldsymbol{\Psi};\boldsymbol{x},t)\, .\mathrm{d}\boldsymbol{\Psi}}. \tag{2}$$

Fluctuations with respect to the Favre average are defined as: $\quad q'' = Q - \widetilde{Q}$.

2.2 Velocity-scalar PDF transport equation

Neglecting the mean viscous stress tensor gradient $\partial\langle\tau_{ij}\rangle / \partial x_j$, the transport equation for the joint velocity-composition MDF $\mathcal{F}_{U\phi}$ reads:

$$\begin{aligned}
&\frac{\partial \mathcal{F}_{U\phi}}{\partial t} + V_j \frac{\partial \mathcal{F}_{U\phi}}{\partial x_j} + \left(-\frac{1}{\langle\rho\rangle}\frac{\partial\langle p\rangle}{\partial x_i} + g_i \right) \frac{\partial \mathcal{F}_{U\phi}}{\partial V_i} + \frac{\partial}{\partial \psi_\alpha}\left[S_\alpha(\boldsymbol{\psi})\, \mathcal{F}_{U\phi} \right] \\
&\quad = -\frac{\partial}{\partial V_i}\Bigg[\underbrace{\left[\left(\frac{1}{\langle\rho\rangle} - \frac{1}{\rho(\boldsymbol{\psi})} \right) \frac{\partial\langle p\rangle}{\partial x_i} + \frac{1}{\rho(\boldsymbol{\psi})} \left\langle -\frac{\partial p'}{\partial x_i} + \frac{\partial \tau'_{ij}}{\partial x_j} \middle| \boldsymbol{V}, \boldsymbol{\psi} \right\rangle \right]}_{\langle a_i |\, \boldsymbol{V},\boldsymbol{\psi}\rangle,\ \text{with } a_i \text{ the GLM}} \mathcal{F}_{U\phi} \Bigg] \\
&\qquad - \frac{\partial}{\partial \psi_\alpha}\Bigg[\underbrace{\frac{1}{\rho(\boldsymbol{\psi})} \left\langle -\frac{\partial J_j^\alpha}{\partial x_j} \middle| \boldsymbol{V}, \boldsymbol{\psi} \right\rangle}_{\langle\, \theta_\alpha |\, \boldsymbol{V},\boldsymbol{\psi}\rangle,\ \text{with } \theta_\alpha \text{ the mixing model}} \mathcal{F}_{U\phi} \Bigg].
\end{aligned} \tag{3}$$

The terms on the left hand side of Eq. (3) appear in closed form: effects of convection and mean pressure gradient are exactly accounted for.

Assumption on flame structure In Eq. (3), the evolution in composition space due to chemical reaction also appears in closed form (last term on the left hand side: chemical source term). In this paper, where the focus is on scalar-flux modelling, we make the assumption that, for the turbulent flames considered, the local structure in composition space corresponds to the composition on the centreline of a laminar diffusion flame in the opposed-jet configuration at a given strain rate. The local composition is then only dependent on one single conserved scalar, the mixture fraction ξ. We use Bilger's definition [8], based on the elements carbon, hydrogen and oxygen:

$$\xi = \frac{\frac{2(Z_\mathrm{C} - Z_{\mathrm{C,o}})}{W_\mathrm{C}} + \frac{Z_\mathrm{H} - Z_{\mathrm{H,o}}}{2W_\mathrm{H}} - \frac{Z_\mathrm{O} - Z_{\mathrm{O,o}}}{W_\mathrm{O}}}{\frac{2(Z_{\mathrm{C,f}} - Z_{\mathrm{C,o}})}{W_\mathrm{C}} + \frac{Z_{\mathrm{H,f}} - Z_{\mathrm{H,o}}}{2W_\mathrm{H}} - \frac{Z_{\mathrm{O,f}} - Z_{\mathrm{O,o}}}{W_\mathrm{O}}}, \tag{4}$$

where Z_β is the total mass fraction of element β and W_β is the atomic mass of element β. The subscripts "f" and "o" refer to the fuel and oxidant streams.

The composition space is reduced to a one-dimensional space and instead of Eq. (3), we model and solve the joint velocity-mixture fraction MDF $\mathcal{F}_{U\xi}(\boldsymbol{V},\zeta;\boldsymbol{x},t)$:

$$\begin{aligned}
\frac{\partial \mathcal{F}_{U\xi}}{\partial t} + V_j \frac{\partial \mathcal{F}_{U\xi}}{\partial x_j} + \left(-\frac{1}{\langle\rho\rangle}\frac{\partial\langle p\rangle}{\partial x_i} + g_i \right) \frac{\partial \mathcal{F}_{U\xi}}{\partial V_i} &= -\frac{\partial}{\partial V_i}\left[\langle a_i |\, \boldsymbol{V},\zeta\rangle \mathcal{F}_{U\xi} \right] \\
&\quad - \frac{\partial}{\partial \zeta}\left[\langle\, \theta_\xi |\, \boldsymbol{V},\zeta\rangle \mathcal{F}_{U\xi} \right],
\end{aligned} \tag{5}$$

where no chemical source term appears (since ξ is a conserved scalar).

2.3 Particle method and Lagrangian modelling

When Eq. (5) is modelled and solved using a particle stochastic approach [1], a set of uniformly distributed computational particles evolves according to stochastic differential equations. Each particle has a set of properties $\{w^\star, m^\star, \boldsymbol{X}^\star, \boldsymbol{u}^\star, \xi^\star\}$ where $w^\star$ is a numerical weight, $m^\star$ is the mass of the particle, $\boldsymbol{X}^\star$ its position, $\boldsymbol{u}^\star$ its fluctuating velocity and $\xi^\star$ the particle's mixture fraction (where the superscript $\star$ denotes that the quantity is a computational particle property). Particle mass $m^\star$ is constant in time.

One can show that solving the following Lagrangian equations for the ensemble of particles:[1]

$$dX_i^\star = U_i^\star dt \qquad \text{with} \qquad U_i^\star = \left[\widetilde{U}_i\right]^\star + u_i^\star, \tag{6}$$

$$d\xi^\star = \theta_\xi^\star dt, \tag{7}$$

$$du_i^\star = -u_j^\star \left[\frac{\partial \widetilde{U}_i}{\partial x_j}\right]^\star dt + \left[\frac{1}{\langle\rho\rangle}\frac{\partial \langle\rho\rangle \widetilde{u_i'' u_j''}}{\partial x_j}\right]^\star dt + a_i^\star dt, \tag{8}$$

where the mean density $\overline{\rho}$ and mean velocity vector $\widetilde{\boldsymbol{U}}$ satisfy the mean continuity and mean momentum equations (neglecting the mean viscous stress tensor gradient):

$$\frac{\partial \overline{\rho}}{\partial t} + \frac{\partial \overline{\rho}\widetilde{U}_j}{\partial x_j} = 0, \tag{9}$$

$$\frac{\partial \overline{\rho}\widetilde{U}_i}{\partial t} + \frac{\partial \overline{\rho}\widetilde{U}_i\widetilde{U}_j}{\partial x_j} = -\frac{\partial \overline{p}}{\partial x_i} - \frac{\partial \overline{\rho}\widetilde{u_i'' u_j''}}{\partial x_j} + \overline{\rho} g_i, \tag{10}$$

is equivalent to solving Eq. (5) for the particle joint velocity-scalar MDF $\mathcal{F}_{U\xi}^P$:

$$\mathcal{F}_{U\xi}^P(\boldsymbol{x}, \boldsymbol{V}, \zeta; t) = \left\langle \sum_\star w^\star m^\star . \delta\big(\boldsymbol{X}^\star(t) - \boldsymbol{x}\big) . \delta\big(\boldsymbol{U}^\star(t) - \boldsymbol{V}\big) . \delta\big(\xi^\star(t) - \zeta\big) \right\rangle. \tag{11}$$

3 Modelling

The Lagrangian model for velocity evolution $a_i^\star$ and the mixing model $\theta_\xi^\star$ close the transport equation for the joint velocity-composition MDF $\mathcal{F}_{U\xi}(\boldsymbol{V}, \zeta; \boldsymbol{x}, t)$, Eq. (5), and therefore imply models for its first statistical moments: the Reynolds stresses $\widetilde{u_i'' u_j''}$ and the scalar fluxes $\widetilde{u_i'' \xi''}$.

3.1 Reynolds-stress model

The Generalised Langevin Model (GLM) [9] is chosen as framework for the stochastic Lagrangian model for particle velocity evolution:

$$a_i^\star dt = \left[G_{ij}\right]^\star u_j^\star dt + \sqrt{C_0 \left[\epsilon\right]^\star} dW_i^\star, \tag{12}$$

[1] The quantities between brackets $[\ ]^\star$ are interpolated at the particle location (obtained by solving the RANS equations (9) and (10) together with the model (15) and a modelled equation for the dissipation rate of turbulent kinetic energy ϵ).

where $dW_i^\star$ is an increment over dt of the Wiener process $W_i^\star$. The matrix G_{ij} reads:

$$G_{ij} = \frac{\epsilon}{k}\left(\alpha_1\delta_{ij} + \alpha_2 b_{ij} + \alpha_3 b_{ij}^2\right) + H_{ijkl}\frac{\partial \widetilde{U}_k}{\partial x_l}, \tag{13}$$

$$\begin{aligned} \text{with} \quad H_{ijkl} &= \beta_1\delta_{ij}\delta_{kl} + \beta_2\delta_{ik}\delta_{jl} + \beta_3\delta_{il}\delta_{jk} \\ &+ \gamma_1\delta_{ij}b_{kl} + \gamma_2\delta_{ik}b_{jl} + \gamma_3\delta_{il}b_{jk} + \gamma_4 b_{ij}\delta_{kl} + \gamma_5 b_{ik}\delta_{jl} + \gamma_6 b_{il}\delta_{jk} \\ &+ \xi_1 b_{ij}b_{kl} + \xi_2 b_{ik}b_{jl} + \xi_3 b_{il}b_{jk}, \end{aligned} \tag{14}$$

where $k = \frac{1}{2}\widetilde{u_k''u_k''}$ is the turbulent kinetic energy and ϵ the modelled turbulent dissipation, such that the choice of the coefficients α_i, β_i, γ_i and ξ_i together with the choice of the coefficient C_0 define the specific form of the GLM (see Table 1 for the definition of the anisotropy tensor b_{ij}).

Table 1 Useful tensors and scalar invariants

$b_{ij} = \frac{\widetilde{u_i u_j}}{\widetilde{u_l u_l}} - \frac{1}{3}\delta_{ij}$	$S_{ij} = \frac{1}{2}\frac{k}{\epsilon}\left(\frac{\partial \widetilde{U}_i}{\partial x_j} + \frac{\partial \widetilde{U}_j}{\partial x_i}\right)$	$I_0 = S_{ll}$	$I_2 = S_{lm}b_{ml}^2$
$b_{ij}^2 = b_{il}b_{lj}$	$W_{ij} = \frac{1}{2}\frac{k}{\epsilon}\left(\frac{\partial \widetilde{U}_i}{\partial x_j} - \frac{\partial \widetilde{U}_j}{\partial x_i}\right)$	$I_1 = S_{lm}b_{ml}$	$I_3 = S_{lm}b_{ml}^3$
$b_{ll}^3 = b_{lk}b_{km}b_{ml}$	$F = 1 - \frac{9}{2}b_{ll}^2 + 9b_{ll}^3$	$\frac{P_k}{\epsilon} = -2\left(I_1 + \frac{1}{3}I_0\right)$	

The implied Reynolds-stress transport equation reads:

$$\frac{\partial \overline{\rho}\widetilde{u_i''u_j''}}{\partial t} + \frac{\partial \overline{\rho}\widetilde{u_i''u_j''}\widetilde{U}_k}{\partial x_k} = -\overline{\rho}\left(\widetilde{u_i''u_k''}\frac{\partial \widetilde{U}_j}{\partial x_k} + \widetilde{u_j''u_k''}\frac{\partial \widetilde{U}_i}{\partial x_k}\right) + \mathcal{T}_{ij} + \overline{\rho}\Pi_{ij} - \frac{2}{3}\epsilon\delta_{ij}, \tag{15}$$

where the implied pressure-strain correlation model Π_{ij} reads:

$$\Pi_{ij} = \left(\frac{2}{3} + C_0\right)\epsilon\delta_{ij} + G_{il}\widetilde{u_l u_j} + G_{jl}\widetilde{u_l u_i}. \tag{16}$$

In this paper, when directly solving Eq. (15) together with Eq. (9) and (10) by means of a Finite-Volume method, we will model the triple correlation term $-\partial\overline{\rho u_i'' u_j'' u_k''}\big/\partial x_k$ using the Daly-Harlow generalised gradient diffusion model:

$$\mathcal{T}_{ij} = -\frac{\partial}{\partial x_k}\left[C_s\overline{\rho}\frac{k}{\epsilon}\widetilde{u_k''u_l''}\frac{\partial \widetilde{u_i''u_j''}}{\partial x_l}\right] \qquad \text{with } C_s = 0.22. \tag{17}$$

This will imply a small difference compared to solving Eq. (5) with the GLM as model for velocity evolution, Eq. (12), since in this case the model for the triple correlation term $\mathcal{T}_{ij}$ directly results from the GLM and is different from Eq. (17) [10].

In the following, we consider the LRR-IPM Reynolds stress model [11] for the pressure-strain correlation Π_{ij}, which can be written in the form:

$$\Pi_{ij} = \epsilon\sum_{n=1}^{5} A^{(n)}T_{ij}^{(n)}, \tag{18}$$

where the nondimensional, symmetric, deviatoric tensors $T_{ij}^{(n)}$ are given in Table 2 and the LRR-IPM coefficients $A^{(n)}$ are given in Table 3.

Table 2 Nondimensional, symmetric, deviatoric tensors $T_{ij}^{(n)}$

$T_{ij}^{(1)} = b_{ij}$	$T_{ij}^{(6)} = S_{il}b_{lj}^2 + S_{jl}b_{li}^2 - \frac{2}{3}I_2\delta_{ij}$
$T_{ij}^{(2)} = b_{ij}^2 - \frac{1}{3}b_{ll}^2\delta_{ij}$	$T_{ij}^{(7)} = W_{il}b_{lj}^2 + W_{jl}b_{li}^2$
$T_{ij}^{(3)} = S_{ij} - \frac{1}{3}I_0\delta_{ij}$	$T_{ij}^{(8)} = b_{il}S_{lm}b_{mj} - \frac{1}{3}I_2\delta_{ij}$
$T_{ij}^{(4)} = S_{il}b_{lj} + S_{jl}b_{li} - \frac{2}{3}I_1\delta_{ij}$	$T_{ij}^{(9)} = b_{il}^2W_{lm}b_{mj} + b_{jl}^2W_{lm}b_{mi}$
$T_{ij}^{(5)} = W_{il}b_{lj} + W_{jl}b_{li}$	$T_{ij}^{(10)} = b_{il}^2S_{lm}b_{mj} + b_{jl}^2S_{lm}b_{mi} - \frac{2}{3}I_3\delta_{ij}$

Table 3 LRR-IPM coefficients $A^{(n)}$

$A^{(1)} = -2C_1$	$A^{(2)} = 0$	$A^{(3)} = \frac{4}{3}C_2$	$A^{(4)} = 2C_2$	$A^{(5)} = 2C_2$

with $C_1 = 1.8$ and $C_2 = 0.6$.

3.2 Mixing models: mean scalar and scalar variance

We usually ask mixing models to satisfy the minimum requirements of conservation of the mean and correct scalar variance decay. These properties are reflected in the transport equations for mean mixture fraction and mixture fraction variance which can be obtained from Eq. (5):

$$\frac{\partial\overline{\rho}\widetilde{\xi}}{\partial t} + \frac{\partial\overline{\rho}\widetilde{U}_j\widetilde{\xi}}{\partial x_j} = -\frac{\partial\overline{\rho}\widetilde{u_j''\xi''}}{\partial x_j} + \underbrace{\overline{\rho\theta_\xi}}_{=0 \text{ (conservation of the mean)}} \tag{19}$$

$$\frac{\partial\overline{\rho}\widetilde{\xi''^2}}{\partial t} + \frac{\partial\overline{\rho}\widetilde{U}_j\widetilde{\xi''^2}}{\partial x_j} + 2\overline{\rho}\widetilde{u_j''\xi''}\frac{\partial\widetilde{\xi}}{\partial x_j} = -\frac{\partial\overline{\rho}\widetilde{u_j''\xi''^2}}{\partial x_j} - \underbrace{2\overline{\rho\xi''\theta_\xi}}_{\text{scalar dissipation rate } \overline{\rho}\widetilde{\chi}} \tag{20}$$

Most mixing models imply a scalar dissipation rate $\widetilde{\chi}$ modelled as: $\widetilde{\chi} = C_\phi\omega\widetilde{\xi''^2}$ (with $\omega = \epsilon/k$). In this paper, we use the value $C_\phi = 2$.

Mixing model dependence on velocity S.B. Pope [13] considered the hypothesis that, at high Reynolds number, the mean of a passive scalar conditional on velocity is independent of the molecular viscosity. This condition is sufficient for the validity of Taylor's idea that the dispersion of a conserved passive scalar is determined by the motion of fluid particles. This is not satisfied by the most widely used mixing models which are independent of velocity. In general, the evolution for the scalar flux $\widetilde{u_j''\xi''}$ and the triple correlation $\widetilde{u_j''\xi''^2}$ in Eq. (19) and (20) depends on the choice of the mixing model.

3.3 Modelled scalar flux

The exact scalar-flux transport equation for high Reynolds number flows reads:

$$\frac{\partial\overline{\rho}\widetilde{u_i''\xi''}}{\partial t} + \frac{\partial\overline{\rho}\widetilde{u_i''\xi''\widetilde{U_j}}}{\partial x_j} + \overline{\rho}\widetilde{u_j''\xi''}\frac{\partial\widetilde{U_i}}{\partial x_j} + \overline{\rho}\widetilde{u_i''u_j''}\frac{\partial\widetilde{\xi}}{\partial x_j} = -\overline{\xi\frac{\partial p}{\partial x_i}} - \frac{\partial\overline{\rho u_i''u_j''\xi''}}{\partial x_j}. \tag{21}$$

Eq. (5) implies the above equation with the following model for the pressure-scrambling term:

$$-\overline{\xi\frac{\partial p}{\partial x_i}} = \overline{\rho}\widetilde{u_i''\theta_\xi} + \overline{\rho}a_i\widetilde{\xi''}. \tag{22}$$

We will suppose that the first term in Eq. (22) takes the form:

$$\overline{\rho}\widetilde{u_i''\theta_\xi} = C_\phi^*\left[\overline{\rho}\frac{\epsilon}{k}\widetilde{u_i''\xi''}\right], \tag{23}$$

with different mixing models possibly leading to different values for C_ϕ^*. It is important to note that for some mixing models which are conditional on velocity this term is zero [12,13] ($C_\phi^* = 0$), as required by Taylor at high Reynolds number. For the widely used IEM model [14,15], $\theta_\xi^\star = -\frac{1}{2}C_\phi\omega(\xi^\star - [\widetilde{\xi}]^\star)$, we can easily see that $C_\phi^* = -\frac{1}{2}C_\phi$. For the Curl's model, S.B. Pope showed in his 1985's paper [1] that $C_\phi^* = -C_\phi$. We will see later in the results for the bluff-body stabilised flame HM1 (Fig. 3) that, in the present case where one single conserved scalar is considered (composition space reduced to a one-dimensional space), the Euclidean minimum spanning tree (EMST) model [16] seems to lead to a C_ϕ^* similar to IEM, while the modified Curl's coalescence dispersion (CD) model [17,18] leads to a higher (absolute) C_ϕ^* value.

With a given mixing model satisfying (23), the GLM-implied model for the pressure-scrambling term reads [2]:

$$-\overline{\xi\frac{\partial p}{\partial x_i}} = -\overline{\rho}\left(-C_\phi^* - \alpha_1\right)\frac{\epsilon}{k}\widetilde{u_i''\xi''} + \overline{\rho}\left(G_{ij} - \alpha_1\frac{\epsilon}{k}\delta_{ij}\right)\widetilde{u_j''\xi''}. \tag{24}$$

This differential scalar-flux model can be compared to the widely used "standard model":

$$-\overline{\xi\frac{\partial p}{\partial x_i}} = -\overline{\rho}C_{\phi1}\frac{\epsilon}{k}\widetilde{u_i''\xi''} + \overline{\rho}C_{\phi2}\widetilde{u_j''\xi''}\frac{\partial\widetilde{U_i}}{\partial x_j}, \tag{25}$$

where the first term is modelled using Monin's model [19] with $C_{\phi1} = 3$, and the second term is the destruction of production model by Launder [20] with $C_{\phi2} = 0.5$.

In a similar way as for the Reynolds stresses in Section 3.1, when directly solving the modelled equation (21) by means of a Finite-Volume method, the triple correlation term $-\partial\overline{\rho u_i'' u_j'' \xi''}\Big/\partial x_j$ will be modelled as:

$$\mathcal{T}_i^\xi = -\frac{\partial}{\partial x_j}\left[C_s^\xi\overline{\rho}\frac{k}{\epsilon}\widetilde{u_j''u_k''}\frac{\partial\widetilde{u_i''\xi''}}{\partial x_k}\right], \quad \text{with } C_s^\xi = 0.22. \tag{26}$$

4 GLM corresponding to given Reynolds-stress and scalar-flux models

We now derive a Langevin model consistent with the LRR-IPM Reynolds-stress model for pressure-strain correlation, and as much as possible consistent with the standard scalar-flux model, Eq. (25).

4.1 GLM general formulation

Table 1 gives a list of useful tensors and scalar invariants. Although we restrict ourselves to the LRR-IPM Reynolds stress model, we will use here a more general formulation, with the modelled pressure-strain correlation expressed in terms of ten tensors $T_{ij}^{(n)}$ as:

$$\Pi_{ij} = \epsilon \sum_{n=1}^{10} A^{(n)} T_{ij}^{(n)}, \tag{27}$$

where the nondimensional, symmetric, deviatoric tensors $T_{ij}^{(n)}$ are given in Table 2. Note that we follow the general formalism introduced in [4], such that the trace of the tensors $T_{ij}^{(n)}$ is zero in variable density flows, and where the tensors $T_{ij}^{(9)}$ and $T_{ij}^{(10)}$ (and the GLM coefficients ξ_i) are introduced in order to allow GLM representations of Reynolds-stress models that include terms which are cubic in b_{ij}. It is useful to write Eq. (13) in terms of the tensors and scalar invariants given in Table 1:

$$\begin{aligned}\frac{k}{\epsilon} G_{ij} = {} & \alpha_1^* \delta_{ij} + \alpha_2^* b_{ij} + \alpha_3 b_{ij}^2 + (\beta_2 + \beta_3) S_{ij} + (\beta_2 - \beta_3) W_{ij} \\ & + (\gamma_2 + \gamma_3) S_{il} b_{lj} + (\gamma_2 - \gamma_3) W_{il} b_{lj} + (\gamma_5 + \gamma_6) b_{il} S_{lj} + (\gamma_5 - \gamma_6) b_{il} W_{lj} \\ & + (\xi_2 + \xi_3) b_{il} S_{lm} b_{mj} + (\xi_2 - \xi_3) b_{il} W_{lm} b_{mj},\end{aligned} \tag{28}$$

where we introduced:

$$\alpha_1^* = \alpha_1 + \beta_1 I_0 + \gamma_1 I_1 \qquad \text{and} \qquad \alpha_2^* = \alpha_2 + \gamma_4 I_0 + \xi_1 I_1. \tag{29}$$

Writing Eq. (16) in the following form:

$$\frac{\Pi_{ij}}{\epsilon} = \left(\frac{2}{3} + C_0\right) \delta_{ij} + 2 \left[\frac{k}{\epsilon} G_{ik} b_{kj} + \frac{k}{\epsilon} G_{jk} b_{ki} + \frac{1}{3} \frac{k}{\epsilon} G_{ij} + \frac{1}{3} \frac{k}{\epsilon} G_{ji}\right], \tag{30}$$

and using the Cayley-Hamilton theorem for the symmetric traceless tensor b_{ij}:

$$b_{ij}^3 = \frac{1}{2} b_{kk}^2 b_{ij} + \frac{1}{3} b_{kk}^3 \delta_{ij}, \tag{31}$$

we finally obtain for the coefficients $A^{(n)}$ defined by Eq. (27) the relations given in Table 4, together with the condition that the term in δ_{ij} should be zero (i.e. that the redistribution term does not affect turbulent kinetic energy):

$$\begin{aligned}0 = {} & \frac{1}{2} + \frac{3}{4} C_0 + \alpha_1^* + \left(\alpha_2^* + \frac{1}{3} \alpha_3\right) b_{kk}^2 + \alpha_3 b_{kk}^3 + \frac{1}{3} (\beta_2 + \beta_3) I_0 \\ & + \left[(\beta_2 + \beta_3) + \frac{1}{3} \gamma^*\right] I_1 + \left[\gamma^* + \frac{1}{3} (\xi_2 + \xi_3)\right] I_2 + [\xi_2 + \xi_3] I_3,\end{aligned} \tag{32}$$

with

$$\gamma^* = \gamma_2 + \gamma_3 + \gamma_5 + \gamma_6. \tag{33}$$

Using the definitions given in Table 1 and the relations given in Table 4, this condition reads:

$$-\left(\frac{1}{2} + \frac{3}{4} C_0\right) + \frac{F}{3} \alpha_2^* = A^*, \tag{34}$$

with

$$A^* = \frac{1}{4}\left[A^{(1)} + A^{(2)}\left(-\frac{1}{2}b_{kk}^2 + 3b_{kk}^3\right) + A^{**}\right], \tag{35}$$
$$A^{**} = A^{(3)}I_0 + 2A^{(4)}I_1 + \left(2A^{(6)} + A^{(8)}\right)I_2 + 2A^{(10)}I_3.$$

Table 4 Relationship between the coefficients $A^{(n)}$ and the GLM parameters

$A^{(1)}$	=	$4\alpha_1^* + \frac{4}{3}\alpha_2^* + 2b_{kk}^2\alpha_3$
$A^{(2)}$	=	$4\alpha_2^* + \frac{4}{3}\alpha_3$
$A^{(3)}$	=	$\frac{4}{3}(\beta_2 + \beta_3)$
$A^{(4)}$	=	$2(\beta_2 + \beta_3) + \frac{2}{3}(\gamma_2 + \gamma_3 + \gamma_5 + \gamma_6)$
$A^{(5)}$	=	$2(\beta_2 - \beta_3) + \frac{2}{3}(\gamma_2 - \gamma_3 - \gamma_5 + \gamma_6)$
$A^{(6)}$	=	$2(\gamma_2 + \gamma_3)$
$A^{(7)}$	=	$2(\gamma_2 - \gamma_3)$
$A^{(8)}$	=	$4(\gamma_5 + \gamma_6) + \frac{4}{3}(\xi_3 + \xi_2)$
$A^{(9)}$	=	$2(\xi_3 - \xi_2)$
$A^{(10)}$	=	$2(\xi_3 + \xi_2)$

As explained in [2], arbitrary values can be chosen for the parameters β_1, γ_1, γ_4 and ξ_1. This is clear from Eq. (29) which shows that their contributions can be incorporated in the coefficients α_1 and α_2 (that can depend on the invariants I_0 and I_1).

Note that the GLM satisfies the condition (see Table 4):

$$\frac{3}{2}A^{(3)} - A^{(4)} + \frac{1}{3}A^{(6)} + \frac{1}{6}A^{(8)} - \frac{1}{9}A^{(10)} = 0. \tag{36}$$

A given Reynolds-stress model needs to satisfy this relation in order to have a GLM representation. This is the case for LRR-IPM (see Table 3). Eq. (36) implies that the expressions for $A^{(3)}$–$A^{(10)}$ in Table 4 only provide seven independent relations for eight parameters: β_2, β_3, γ_2, γ_3, γ_5, γ_6, ξ_2 and ξ_3. Introducing the parameter β^*:

$$\beta^* = \frac{1}{4}A^{(5)} - \frac{1}{12}A^{(7)} - \frac{1}{24}A^{(8)} + \frac{1}{36}A^{(10)} + \frac{1}{3}\gamma_5, \tag{37}$$

we can express the parameters β_2, β_3, γ_2, γ_3, γ_5, γ_6, ξ_2, ξ_3 of the GLM as function of the coefficients $A^{(3)}$–$A^{(10)}$ (see Table 5). The value $\beta^* = \frac{1}{2}$ was proposed since it leads to $\beta_2 - \beta_3 = 1$ as required in isotropic turbulence [9,2].

In order to determine the remaining GLM coefficients α_1, α_2, α_3 and C_0, we use the relations for $A^{(1)}$ and $A^{(2)}$ from Table 4, together with the condition that the redistribution term does not affect the turbulent kinetic energy, Eq. (34).

A fourth relation is needed. We will now briefly review the case when C_0 is given a constant value (which corresponds to the implementation of the GLM which has been used so far in the tranported PDF computer code 'PDFD' originally developed at TU Delft [10]). We will then come to the new idea of this paper: to provide the fourth condition by specifying the linear relaxation constant in the GLM-implied scalar-flux model. We will see the influence of the value for β^* on the modelling of the rapid-pressure-scrambling term.

Table 5 Relationship between the GLM H_{ijkl}-tensor parameters and the coefficients $A^{(n)}$

β_1	=	arbitrary
γ_1	=	arbitrary
γ_4	=	arbitrary
ξ_1	=	arbitrary
β_2	=	$\frac{3}{8}A^{(3)} + \beta^*$
β_3	=	$\frac{3}{8}A^{(3)} - \beta^*$
γ_2	=	$\frac{1}{4}\left(A^{(6)} + A^{(7)}\right)$
γ_3	=	$\frac{1}{4}\left(A^{(6)} - A^{(7)}\right)$
γ_5	=	from Eq. (37), after choosing an arbitrary value for β^*
γ_6	=	$\frac{1}{4}A^{(8)} - \frac{1}{6}A^{(10)} - \gamma_5$
ξ_2	=	$\frac{1}{4}\left(A^{(10)} - A^{(9)}\right)$
ξ_3	=	$\frac{1}{4}\left(A^{(10)} + A^{(9)}\right)$

4.2 GLM formulations with constant or variable C_0

By setting a constant value for C_0, from the expressions for $A^{(1)}$ and $A^{(2)}$ given in Table 4 and Eq. (34), we can obtain the parameters α_1^*, α_2^* and α_3:

$$\alpha_2^* = \frac{3}{F}\left[\left(\frac{1}{2} + \frac{3}{4}C_0\right) + A^*\right], \tag{38}$$

$$\alpha_3 = \frac{3}{4}A^{(2)} - 3\alpha_2^*, \tag{39}$$

$$\alpha_1^* = \frac{1}{4}A^{(1)} - \frac{1}{3}\alpha_2^* - \frac{1}{2}b_{kk}^2\alpha_3, \tag{40}$$

This form is proposed by S.B. Pope in [2], with $C_0 = 2.1$ (and $\beta^* = \frac{1}{2}$, as mentioned above). As explained in [2], the occurrence of $1/F$ in the expression for α_2 raises the question of realisability when F goes to zero (when a two-component state is approached). Such situations do not occur in the calculations presented in this paper. Nevertheless, the implementation of the GLM corresponding to the LRR-IPM is done in such a way that if F is close to zero, it is substituted by the LIPM model [2]. In this case, $C_0 = 2.1$ and the value for α_2 is fixed to $\alpha_2 = 3.5$; α_3 is obtained from Eq. (39), α_1 is deduced from the redistribution condition (33) and $A^{(1)}$ from Table 4.

The coefficient C_0 in the GLM was first identified as a Kolmogorov constant (from considerations on the Lagrangian velocity structure function which should be isotropic and linear in the dissipation rate in the inertial range). The choice of the value $C_0 = 2.1$ was determined by Anand and Pope [21] by considering the evolution of the thermal wake behind a line source in grid turbulence (moderate Reynolds number). In order to calibrate this constant value, velocity evolution was modelled using the simplified Langevin model together with an equation for position evolution corresponding to a diffusing particle (i.e. including first-order effects of molecular diffusion). Recently, Viswanathan and Pope came back to such studies of dispersion from line sources [22], also comparing to experimental data from moderate Reynolds number flows. They mostly used the constant value $C_0 = 2.1$ but also obtained good results with the constant value $C_0 = 3$. The value of C_0 is Reynolds number dependent: it increases with the Reynolds number and approaches an asymptotic value $C_0(\infty)$ [23]. The value $C_0 = 2.1$ obtained for a moderate Reynolds number flow is probably two to three times lower than the value $C_0(\infty)$ in high Reynolds number flows [24]. It was also observed

that some anisotropy in the Lagrangian velocity structure function could be important in shear flows [25]. This was also considered in [26] where the effects of anisotropy together with acceleration fluctuations on the variations in $C_0(\infty)$ were discussed. The choice for a constant value of C_0 is therefore questionable.

Other forms of the GLM have been proposed where C_0 is not a constant. For instance the IPMb model, corresponding to the LRR-IPM Reynolds-stress model, proposed in [2] and in [3], reads:

$$\alpha_2^* = \alpha_3 = 0, \;\; \alpha_1^* = \frac{1}{4}A^{(1)} \;\text{ and }\; C_0 = \frac{4}{3}\left(-\frac{1}{2} - A^*\right) = \frac{2}{3}\left(-1 + C_1 + C_2\frac{P_k}{\epsilon}\right). \quad (41)$$

Here we introduced the production of turbulent kinetic energy $P_k = -2\epsilon\left(I_1 + \frac{1}{3}I_0\right)$. In this case, the realisability constraint is $C_0 \geq 0$. This condition can be satisfied by specifying the first LRR-IPM model constant as [3]: $C_1 = \max\left[1.8; 1 - C_2\frac{P_k}{\epsilon}\right]$.

4.3 GLM formulation consistent with standard scalar-flux model

The standard pressure-scrambling model, given in Eq. (25), can be written:

$$-\overline{\xi\frac{\partial p}{\partial x_i}} = \overline{\rho}\widetilde{u_j''\xi''}\frac{\epsilon}{k}\left[-C_{\phi 1}\delta_{ij} + C_{\phi 2}\left(S_{ij} + W_{ij}\right)\right]. \quad (42)$$

Using Eq. (24) and (28), the GLM-implied model for the pressure-scrambling term reads:

$$-\overline{\xi\frac{\partial p}{\partial x_i}} = \overline{\rho}\widetilde{u_j''\xi''}\frac{\epsilon}{k}\;\Big[\left(C_\phi^* + \alpha_1^*\right)\delta_{ij} + \left(\alpha_2^* b_{ij} + \alpha_3 b_{ij}^2\right) + \beta_2\left(S_{ij} + W_{ij}\right) + \beta_3\left(S_{ij} - W_{ij}\right) + \Lambda_{ij}\Big], \quad (43)$$

where the terms in α_2^* and α_3 correspond to non-linear relaxation of the scalar flux (i.e. anisotropy effects in the scalar-flux decay rate), and where Λ_{ij} includes other higher-order contributions:

$$\begin{aligned}\Lambda_{ij} = {} & \left(\gamma_2 + \gamma_3\right) S_{il}b_{lj} + \left(\gamma_5 + \gamma_6\right) S_{jl}b_{li} + \left(\gamma_2 - \gamma_3\right) W_{il}b_{lj} - \left(\gamma_5 - \gamma_6\right) W_{jl}b_{li} \\ & + \left(\xi_2 + \xi_3\right) b_{il}S_{lm}b_{mj} + \left(\xi_2 - \xi_3\right) b_{il}W_{lm}b_{mj}. \end{aligned} \quad (44)$$

Perfect match between GLM-implied model and standard model? In order to have an exact correspondence of the GLM-implied model with the standard model, the terms in α_2^* and α_3 in the slow term, and the β_3 and Λ_{ij} terms in the rapid term should vanish in Eq. (43). Moreover, we should require: $\alpha_1^* = -C_{\phi 1} - C_\phi^*$ and $\beta_2 = C_{\phi 2}$.

For some Reynolds-stress models the Λ_{ij} contribution is not zero, which already prevents an exact correspondence. Let's consider the LRR-IPM model, for which this contribution is zero. In order to remove the term in β_3 in Eq. (43), we can specify $C_{\phi 2} = \frac{3}{4}A^{(3)}$, such that $\beta_3 = 0$. The LRR-IPM can lead to the standard rapid term by setting the constant value $C_{\phi 2} = 0.6$ (which implies setting the value $\beta^* = 0.3$ in the GLM). It is more problematic to match the slow term. The IPMb model mentioned above, can remove the non-linear relaxation contributions in the slow term since $\alpha_2^* = \alpha_3 = 0$. However, the typical value for the Monin constant $C_{\phi 1} = 3$ is quite different from $-\alpha_1^* = 0.9$ given by the IPMb. Only the effect of the mixing model ($C_\phi^* \neq 0$) can help to get the correspondence (in this case with $C_\phi^* = -2.1$). This is of course

not satisfactory, since at high Reynolds number, mixing models should ideally lead to $C_\phi^* = 0$, in agreement with Taylor's idea.

Since the "perfect match", with $C_\phi^* = 0$, is not possible, we consider a GLM formulation that is consistent with the standard scalar-flux model for the linear relaxation term and for the mean velocity gradient contributions in the rapid term (β_2 and β_3 terms), requiring $\alpha_1^* = -C_{\phi 1} - C_\phi^*$ and $\beta_2 = C_{\phi 2}$, and where the effect of the mixing model ($C_\phi^* \neq 0$) is included in the non-linear relaxation terms.

Rapid-pressure-scrambling term In order to ensure that $\beta_2 = C_{\phi 2}$, we simply specify:

$$\beta^* = C_{\phi 2} - \frac{3}{8} A^{(3)}. \tag{45}$$

For most Reynolds-stress models where the same value $A^{(3)} = \frac{4}{5}$ is fixed according to the rapid distortion theory, using the value $C_{\phi 2} = 0.5$, we obtain $\beta^* = 0.2$ instead of the originally proposed value $\beta^* = 0.5$. In this pragmatic approach, it is the modelling of the rapid-pressure-scrambling term in the GLM-implied scalar-flux equation that determines the value of β^*.

We chose here to take the rapid-pressure-scrambling term of Launder as a reference since it is a widely used model. However, we should recall that the value $\beta^* = 0.5$ required in isotropic turbulence implies the β_2 and β_3 terms in Eq. (43) as proposed by Lumley [2,27].

Monin's term For the relaxation term, the condition $\alpha_1^* = -C_{\phi 1} - C_\phi^*$ together with the first relations in Table 4 imply:

$$\alpha_2^* = \frac{3}{\left(1 - \frac{9}{2} b_{kk}^2\right)} \left[\left(C_{\phi 1} + C_\phi^*\right) + \frac{1}{4} A^{(1)} - \frac{3}{8} b_{kk}^2 A^{(2)} \right]. \tag{46}$$

The factor $1 - \frac{9}{2} b_{kk}^2$ in the above equation implies a singularity at $b_{kk}^2 = \frac{2}{9}$, values that can occur within the Lumley triangle [7,27] (i.e. values that can occur for realisable values of the Reynolds stresses). Using the representation of the Lumley triangle used by S.B. Pope in [7], the line $b_{kk}^2 = \frac{2}{9}$ is shown in Fig. 2.

The following alternative way of writing the GLM-implied pressure-scrambling term (43) obtained by introducing the Cayley-Hamilton relation (31), permits to have the factor F instead of the factor $1 - \frac{9}{2} b_{kk}^2$ in the expression for α_2^*:

$$\begin{aligned} -\xi \overline{\frac{\partial p}{\partial x_i}} = \overline{\rho} \widetilde{u_j'' \xi''} \frac{\epsilon}{k} \Bigg[& \left(C_\phi^* + \alpha_1^* + \alpha_3 b_{kk}^3 \right) \delta_{ij} + \left(\alpha_2^* + \frac{3}{2} \alpha_3 b_{kk}^2 \right) b_{ij} + \alpha_3 \left(b_{ij}^2 - 3 b_{ij}^3 \right) \\ & + \beta_2 \left(S_{ij} + W_{ij} \right) + \beta_3 \left(S_{ij} - W_{ij} \right) + \Lambda_{ij} \Bigg]. \end{aligned} \tag{47}$$

This way to write the GLM-implied model is simply a reinterpretation of the relaxation terms. Requiring $\alpha_1^* = -C_{\phi 1} - C_\phi^* - \alpha_3 b_{kk}^3$ now leads to:

$$\alpha_2^* = \frac{3}{F} \left[\left(C_{\phi 1} + C_\phi^*\right) + \frac{1}{4} A^{(1)} + \frac{3}{4} \left(\frac{-1}{2} b_{kk}^2 + b_{kk}^3 \right) A^{(2)} \right], \tag{48}$$

$$\alpha_3 = \frac{3}{4} A^{(2)} - 3 \alpha_2^*, \tag{49}$$

$$\alpha_1^* = -C_{\phi 1} - C_\phi^* - \alpha_3 b_{kk}^3, \tag{50}$$

$$C_0 = \frac{4}{3} \left[\left(C_{\phi 1} + C_\phi^*\right) - \frac{1}{2} - \frac{1}{4} \left(A^{(2)} b_{kk}^2 + A^{**} \right) \right], \tag{51}$$

where C_0 was obtained from Eq. (34).

In the case of isotropic turbulence for a constant density flow, and for $C_\phi^* = 0$, we obtain the value $C_0 = \frac{10}{3} \approx 3.33$. Note that if the IEM model is used with $C_\phi = 2$ (i.e. $C_\phi^* = -1$), we obtain a value $C_0 = 2.0$ which is close to the constant value $C_0 = 2.1$ proposed by Anand and Pope. This suggests that so far, in transported joint velocity-composition PDF calculations, the too low value $C_0 = 2.1$ together with the typical non-zero values for C_ϕ^*, have implied scalar-flux models where the modelling of the relaxation term resulted to be in good correspondence with Monin's model with standard constant value.

The main advantage of the GLM coefficients given by Eq. (48)-(51) is that they lead to a scalar-flux model in more complete correspondence with standard models:

$$-\overline{\xi \frac{\partial p}{\partial x_i}} = \overline{\rho} \widetilde{u_j'' \xi''} \frac{\epsilon}{k} \left[\left(-C_{\phi 1} - \alpha_3 b_{kk}^3 \right) \delta_{ij} + \left(\alpha_2^* b_{ij} + \alpha_3 b_{ij}^2 \right) \right. \\ \left. + C_{\phi 2} \left(S_{ij} + W_{ij} \right) + \left(\frac{3}{4} A^{(3)} - C_{\phi 2} \right) \left(S_{ij} - W_{ij} \right) + \Lambda_{ij} \right], \tag{52}$$

where the effect of the mixing model through C_ϕ^* appears in the non-linear relaxation α_2^* and α_3 terms. In this case, it is the modelling of Monin's term which determines the value of the coefficient C_0.

Realisability For the LRR-IPM:

$$C_0 = \frac{2}{3} \left[-1 + 2 \left(C_{\phi 1} + C_\phi^* \right) + C_2 \frac{P_k}{\epsilon} \right]. \tag{53}$$

It is interesting to notice that this expression is similar to the expression from the IPMb model (41), where the constant $2(C_{\phi 1} + C_\phi^*)$ appears instead of C_1. The realisability condition $C_0 \geq 0$ can be written $\frac{P_k}{\epsilon} \geq -\frac{25}{3}$ which is bound to be satisfied (compared to $\frac{P_k}{\epsilon} \geq -\frac{4}{3}$ for IPMb). Still, following the idea of [3] for IPMb, in order to make sure that realisability is statisfied, the constant $C_{\phi 1}$ can be adjusted by specifying $C_{\phi 1} = \max \left[3.0; \frac{1}{2} - \frac{C_2}{2} \frac{P_k}{\epsilon} - C_\phi^* \right]$.

On the other hand, we still have the occurrence of the factor $1/F$ in the expression for α_2^*. This issue is not considered here since for the turbulent flame considered in this paper all the points in the calculation are away from a two-component state ($F = 0$), as can be seen in Fig. 2.

5 Results

The test case considered is the bluff-body stabilised flame HM1 [5,6] which is a target flame of the International Workshop on Measurement and Computation of Turbulent Nonpremixed Flames (TNF workshop) [28]. The numerical settings (grid, boundary conditions) are as in [10]. In the following, D_b and R_b refer respectively to the diameter and radius of the bluff-body: $D_b = 5$cm and $R_b = 2.5$cm. Table 6 summarises the different calculations which will be discussed in the following.

Table 6 Summary of the calculations

	Method	Submodels		Figures
A1	JVSPDF, Eq. (5)	IEM, $C_\phi = 2$	new GLM, Eq. (48)-(51)	1, 2, 4, 5
B	JVSPDF, Eq. (5)	IEM, $C_\phi = 2$	GLM, Eq. (38)-(40), $C_0 = 2.1$	3
C	JVSPDF, Eq. (5)	CD, $C_\phi = 2$	GLM, Eq. (38)-(40), $C_0 = 2.1$	3
D	JVSPDF, Eq. (5)	EMST, $C_\phi = 2$	GLM, Eq. (38)-(40), $C_0 = 2.1$	3
A2	Eq. (19)-(21)	Eq. (24), $C_\phi^* = -1$	with Eq. (26) & Eq. (48)-(50)	5, 6
A3	Eq. (19)-(21)	Eq. (25)	with Eq. (26)	6

All calculations use LRR-IPM model with modified constant $C_{\epsilon 1} = 1.6$. Calculations A2 and A3 are performed using the mean flow field and mean density field from calculation A1.

5.1 Flow fields

From the comparative study presented in [29] for the bluff-body flame HM1, the LRR-IPM Reynolds-stress model is used with the modified constant value $C_{\epsilon 1} = 1.6$. Figure 1 shows that the mean flow field is reasonably well predicted as in [29,10]. As reported in [30] (not shown here), the choice of the scalar-flux model or whether assumed-shape PDF or transported PDF methods are used has almost no influence on the flow field results (since the resulting differences in mean density are small and do not have influence on the mean flow field through the mean continuity equation).

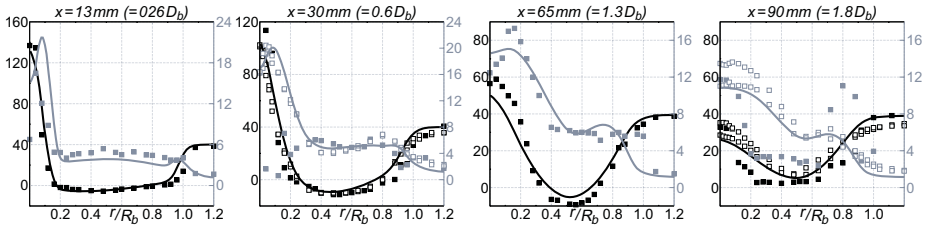

Fig. 1 Radial profiles of mean axial velocity $\widetilde{U}$ (black / left axis) and fluctuating axial velocity $\sqrt{\widetilde{u''^2}}$ (grey / right axis) for the bluff-body flame HM1, in m/s. Filled symbols: measurements in flame HM1. Empty symbols: measurements in flame HM1e. Lines: calculation A1.

For realisability considerations it is interesting to plot all the computed points in the Lumley triangle. In Fig. 2, we see that all the points are far from a two-component state (far from the $F = 0$ line).

5.2 GLM with constant C_0: influence of the mixing model on mean scalar

We illustrate here how the GLM implementation with constant $C_0 = 2.1$ given by Eq. (38)-(40) makes the mean scalar field results dependent on the choice of the mixing model (i.e. on C_ϕ^*). This dependence of the mean scalar on the mixing model comes from the difference in scalar-flux modelling as shown in Eq. (24).

In Fig. 3, we observe that, in this case where one single conserved scalar is considered, IEM and EMST mixing models lead to similar results for mean mixture fraction, while the CD mixing model leads to different results (higher mean mixture fraction on the centreline). A similar observation can be made from one figure presented in [31]

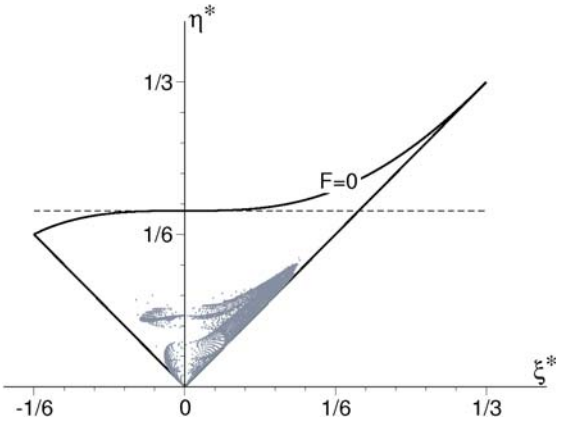

Fig. 2 The Lumley triangle represented using the invariants ξ^* and η^* as in [7]. The dotted line corresponds to $b_{kk}^2 = \frac{2}{9}$. The grey dots correspond to the calculated values in the computational domain for the bluff-body stabilised flame HM1 using LRR-IPM.

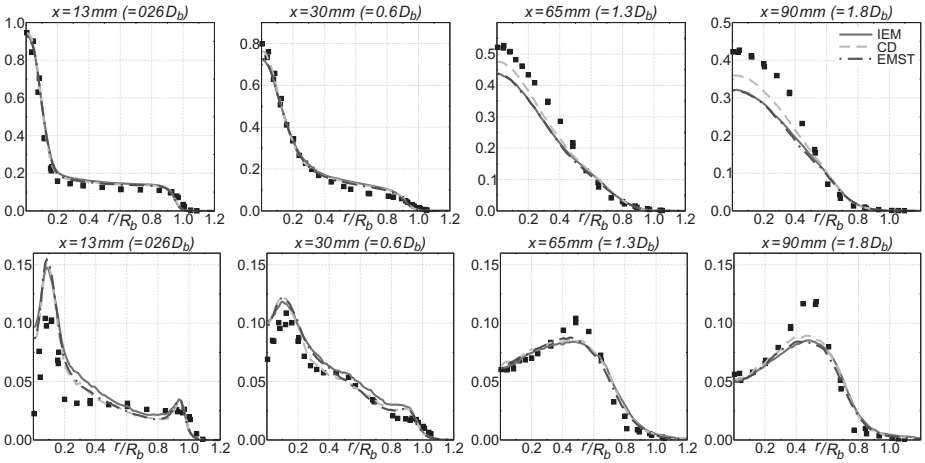

Fig. 3 Radial profiles of mixture fraction for Sydney bluff-body stabilised flame HM1. Top: mean / Bottom: fluctuation (rms). Symbols: measurements. Lines: transported joint velocity-scalar PDF calculations with $C_\phi = 2$ (calculations B, C and D in Table 6).

(Fig. 9), showing mean mixture fraction axial profiles on the centerline using the three mixing models for a turbulent lifted flame. Note that, to the best of the authors' knowledge, this is the only figure in the literature showing a comparison of different transported velocity-scalar PDF results for a mean scalar using different mixing models while the other submodels and model constants are fixed.

The IEM and EMST mixing models move the composition of the computational particles to neighbouring values, while the CD mixing model allows particles with a given velocity to "jump" in composition space. We can expect the latter to induce more decorrelation between velocity components and scalars, which corresponds to a larger negative value for C_ϕ^* (and a larger value for the implied Monin constant). Note that for this flame, a mixing model conditional on the velocity satisfying $C_\phi^* = 0$ would lead

to poor predictions of the mean mixture fraction, due to a too low implied value for the Monin constant.

Only small differences are observed for mixture fraction variance. This is probably due to the fact that the differences in velocity-scalar correlation are small compared to the scalar dissipation rate which is modelled in the same way by the different mixing models.

5.3 Proposed GLM: results with implied scalar-flux model

Fig. 4 shows radial profiles of the coefficient C_0 obtained in a tranported PDF calculation using the newly proposed GLM and the IEM mixing model with $C_\phi = 2$ (calculation A1 in Table 6). We see that in the shear layers the value is larger than the value $C_0 = 2.0$ corresponding to constant-density homogeneous isotropic turbulence. It is quite remarkable that in this case (IEM mixing model with $C_\phi = 2$), the values for C_0 are not too different from the constant value $C_0 = 2.1$.

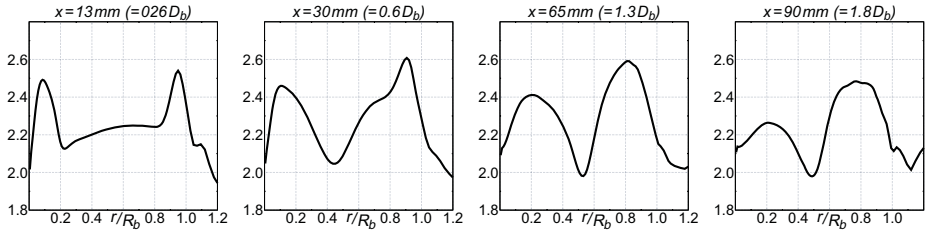

Fig. 4 Radial profiles of C_0 for Sydney bluff-body stabilised flame HM1 (calculation A1 in Table 6).

Figure 5 shows the results for mean mixture fraction and mixture fraction variance obtained in two different ways with the proposed GLM-implied model for the pressure-scrambling term in the scalar-flux modelling. On the one hand, mean particle fields are extracted from a transported PDF calculation using the newly proposed GLM and the IEM mixing model with $C_\phi = 2$ (A1 in Table 6). On the other hand, using the same mean density and flow fields, the GLM-implied model is solved using a Finite-Volume method (A2 in Table 6). The differences in the results may come from the differences in triple correlation modelling, or from numerical errors. We know from scalar PDF results obtained with the same computer code, for instance from the calculations presented in [32], where the same gradient diffusion model is applied both in Finite-Volume and particle methods that the numerical errors only lead to small differences in the results. Therefore, the differences observed in Figure 5, especially for mixture fraction variance, are mainly attributed to the differences in triple correlation modelling: Eq. (26) for the GLM-implied calculation A2 and a model resulting from the combination of the GLM and the mixing model for the tranported PDF calculation A1.

Finally, we check the consistency between the proposed GLM-implied model and the standard model (respectively from calculations A2 and A3 in Table 6). In both cases, equations for mean mixture fraction, variance and scalar fluxes are solved using a Finite-Volume method, using Eq. (26) in order to model the triple correlation, with the mean density and flow fields from the transported PDF calculation. The difference

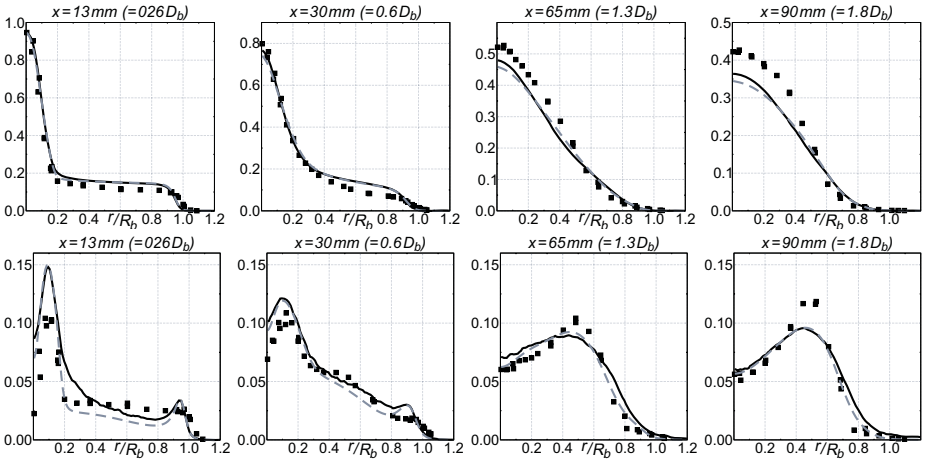

Fig. 5 Radial profiles of mixture fraction for Sydney bluff-body stabilised flame HM1. Top: mean / Bottom: fluctuation (rms). Symbols: measurements. Solid black line: transported PDF, calculation A1. Dashed grey line: GLM-implied model, calculation A2.

in the results may come from the anisotropy effects in the relaxation term or from the β_3 term in the rapid-pressure-scrambling contribution, as discussed at the beginning of Section 4.3. We actually see no difference in the results in the first downstream radial profiles for mean mixture fraction and mixture fraction variance (not shown). Only at a downstream distance $x = 120$mm, some small differences can be observed, as shown in Fig. 6, showing that the proposed GLM indeed implies a pressure-scrambling model in close correspondence with the chosen standard scalar-flux model.

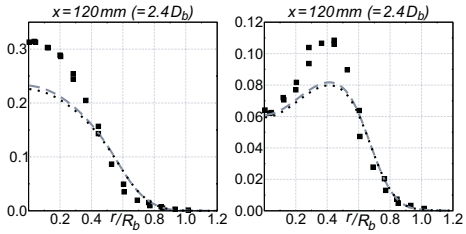

Fig. 6 Radial profiles of mixture fraction for Sydney bluff-body stabilised flame HM1. Left: mean / Right: fluctuation (rms). Symbols: measurements. Dashed grey line: GLM-implied model, calculation A2. Dotted black line: standard model, calculation A3.

6 Conclusions

We derived a GLM formulation with non-constant diffusion coefficient C_0 in close correspondence with a widely used standard differential scalar-flux second-moment closure. The correspondence is not exact since the GLM-implied model includes anisotropy effects in the relaxation term and extra contributions in the rapid-pressure-scrambling term. We verified for the Sydney bluff-body stabilised flame HM1 that results are indeed

identical using either the standard model or the GLM-implied model (with LRR-IPM Reynolds-stress model). The derivation was done using a general formalism such that it can be applied to different Reynolds-stress or scalar-flux models that have a GLM representation.

It was shown that in GLM formulations with constant C_0 the scalar-flux model depends on the choice of the mixing model, when $C_\phi^* \neq 0$ (which is the case for the most widely used mixing models which are independent of velocity). In principle, there is no reason why such formulations should imply scalar-flux models in correspondence with the standard model. However, it appears that the constant value $C_0 = 2.1$ together with the typical C_ϕ^* values of the widely used mixing models ($C_\phi^* = -\frac{1}{2}C_\phi$ or $C_\phi^* = -C_\phi$ with $C_\phi = 2$) yields a Monin term in the scalar-flux model which is not too different from the standard model. Therefore, the forms of the GLM with constant C_0 used so far in transported joint velocity-scalar PDF calculations have lead to scalar-flux models in reasonably good correspondence with the standard model, thanks to the effect of the mixing model. However, they would lead to quite different scalar-flux modelling if the mixing model used would satisfy $C_\phi^* = 0$.

In the proposed GLM formulation, the value of the coefficient C_0 is determined such that the required relaxation for the Monin term in the implied scalar-flux model is prescribed. Moreover, by knowing the C_ϕ^* value of the chosen mixing model, the dependency of the GLM-implied scalar-flux model on the mixing model is removed for the linear relaxation term. The modelling of the rapid-pressure-scrambling term is related to the value of the GLM parameter β^*. The constant value $C_{\phi 2} = 0.5$ for Launder's destruction of production's model, together with assumptions from the rapid distortion theory used to fix the Reynolds-stress model constant $A^{(3)} = \frac{4}{5}$, would lead to $\beta^* = 0.2$ instead of the originally proposed value $\beta^* = 0.5$ based on considerations from isotropic turbulence.

Acknowledgements This collaborative research is supported by the Comunidad de Madrid through Project HYSYCOMB, P2009/ENE-1597, by the Spanish Ministry of Science and Innovation under Project ENE2008-06515-C04-02, and by the Fund of Scientific Research – Flanders (Belgium) (FWO-Vlaanderen) through FWO-project G.0079.07.

References

1. S.B. Pope. PDF methods for turbulent reactive flows. *Progress in Energy and Combustion Science*, 11:119-192, 1985.
2. S.B. Pope. On the relationship between stochastic Lagrangian models of turbulence and second-moment closures. *Physics of Fluids*, 6:973-985, 1994.
3. P.A. Durbin and C.G. Speziale. Realizability of second-moment closure via stochastic analysis *Journal of Fluid Mechanics*, 280:395-407, 1994.
4. H.A. Wouters, T.W.J. Peeters and D. Roekaerts. On the existence of a Generalized Langevin model representation for second-moment closures. *Physics of Fluids*, 8:1702-1704, 1996.
5. B.B. Dally and A.R. Masri. Flow and mixing fields of turbulent bluff-body jets and flames. *Combustion Theory and Modelling*, 2:193-219, 1998.
6. B.B. Dally, A.R. Masri, R.S. Barlow and G.J. Fiechtner. Instantaneous and mean compositional structure of bluff-body stabilized nonpremixed flames. *Combustion and Flame*, 114:119-148, 1998.
7. S.B. Pope. *Turbulent Flows*, Cambridge University Press, 2000.
8. R.W. Bilger, S.H. Starner and R.J. Kee. On reduced mechanisms for methane-air combustion in nonpremixed flames. *Combustion and Flame*, 80:135-149, 1990.
9. D.C. Haworth and S.B. Pope. A generalized Langevin model for turbulent flows. *Physics of Fluids*, 29:387-405, 1986.

10. B. Naud, C. Jiménez and D. Roekaerts. A consistent hybrid PDF method: implementation details and application to the simulation of a bluff-body stabilised flame. *Progress in Computational Fluid Dynamics*, 6:146-157, 2006.
11. B.E. Launder, G.J. Reece and W. Rodi. Progress in the development of a Reynolds-stress turbulence closure. *Journal of Fluid Mechanics*, 68:537-566, 1975.
12. R.O. Fox. On velocity-conditioned scalar mixing in homogeneous turbulence. *Physics of Fluids*, 8:2678-2691, 1996.
13. S.B. Pope. The vanishing effect of molecular diffusivity on turbulent dispersion: implications for turbulent mixing and the scalar flux. *Journal of Fluid Mechanics*, 359:299-312, 1998.
14. J. Villermaux and J.C. Devillon. In *Proc. Second Int. Symp. On Chemical Reaction Engineering*, New York, Elsevier, 1972.
15. C. Dopazo and E.E. O'Brien. An approach to the autoignition of a turbulent mixture. *Acta Astronautica*, 1:1239-1266, 1974.
16. S. Subramaniam and S.B. Pope. A Mixing model for turbulent reactive flows based on Euclidian Minimum Spanning Trees. *Combustion and Flame*, 115:487-514, 1998.
17. J. Janicka, W. Kolbe and W. Kollmann. Closure of the transport equation for the probability density function of turbulent scalar fields. *Journal Non-Equilibrium Thermodynamics*, 4:47-66, 1979.
18. H.A. Wouters, T.W.J. Peeters and D. Roekaerts. Joint velocity-scalar PDF methods. Chapter 2 in *Closure strategies for turbulent and transitional flows (Edited by B. Launder and N. Sandham)*, pp. 626-655, Cambridge University Press, 2002.
19. A.S. Monin. On the symmetry properties of turbulence in the surface layer of air. *IZV Atm. Oceanic, Phys.*, 1:45-54, 1965.
20. B.E. Launder. Heat and mass transport. In *Turbulence, (Edited by P. Bradshaw), Topics in Applied Physics*, 12:231-287, Springer, 1978.
21. M.S. Anand and S.B. Pope. Diffusion behind a line source in grid turbulence. In *Turbulent Shear Flows 4 (Edited by L.J.S. Bradbury, F. Durst, B.E. Launder, F.W. Schmidt and J.H. Whitelaw*), p. 46, Springer-Verlag, Berlin, 1985.
22. S. Viswanathan and S.B. Pope. Turbulent dispersion from line sources in grid turbulence. *Physics of Fluids*, 20:1-25, 2008.
23. B.L. Sawford. Reynolds number effects in Lagrangian stochastic models of turbulent dispersion. *Physics of Fluids A*, 3:1577-1586, 1991.
24. S.B. Pope. Lagrangian PDF methods for turbulent flows. *Annu. Rev. Fluid Mech.*, 26:23-63, 1994.
25. S.B. Pope. Stochastic Lagrangian models of velocity in homogeneous turbulent shear flow. *Physics of Fluids*, 14:1696-1702, 2002.
26. S. Heinz On the Kolmogorov constant in stochastic turbulence models. *Physics of Fluids*, 14:4095-4098, 2002.
27. J.L. Lumley. Computational modeling of turbulent flows. *Advances in Applied Mechanics*, 18:123-176, 1978.
28. R.S. Barlow. International Workshop on Measurement and Computation of Turbulent Nonpremixed Flames. http://www.ca.sandia.gov/TNF
29. G. Li, B. Naud and D. Roekaerts. Numerical Investigation of a Bluff-Body Stabilised Nonpremixed Flame with Differential Reynolds-Stress Models. *Flow, Turbulence and Combustion*, 70:211-240, 2003.
30. B. Naud, R. De Meester, B. Merci and D. Roekaerts. Velocity-scalar correlation modelling in turbulent nonpremixed flames: standard second-moment closure and joint velocity-scalar transported PDF modelling. In *THMT'09 Proceedings of the International Symposium Turbulence, Heat and Mass Transfer 6 (CD-ROM Edited by K. Hanjalić, Y. Nagano and S. Jakirlić)*, 12 pages, Begell House Inc., 2009.
31. R.R. Cao, S.B. Pope, A.R. Masri, Turbulent lifted flames in a vitiated coflow investigated using joint PDF calculations. *Combustion and Flame*, 142:438-453, 2005.
32. B. Merci, D. Roekaerts, B. Naud, S.B. Pope. Comparative study of micromixing models in transported scalar PDF simulations of turbulent nonpremixed bluff body flames. *Combustion and Flame*, 146:109-130, 2006.

Figure 1

Click here to download line figure: HM1_U_u.eps

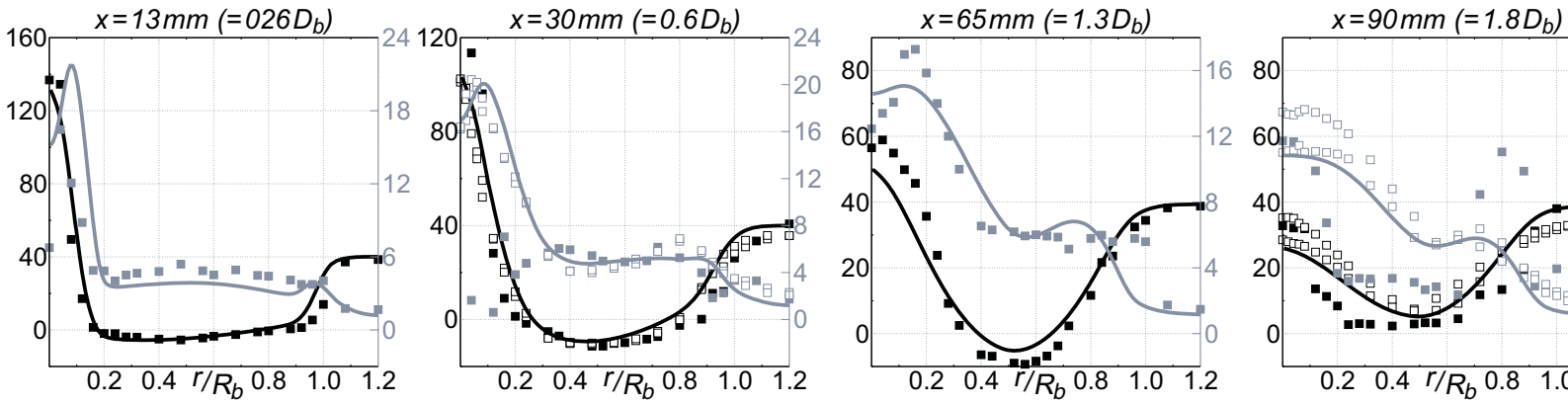

Figure 2
Click here to download line figure: Lumley_triangle.eps

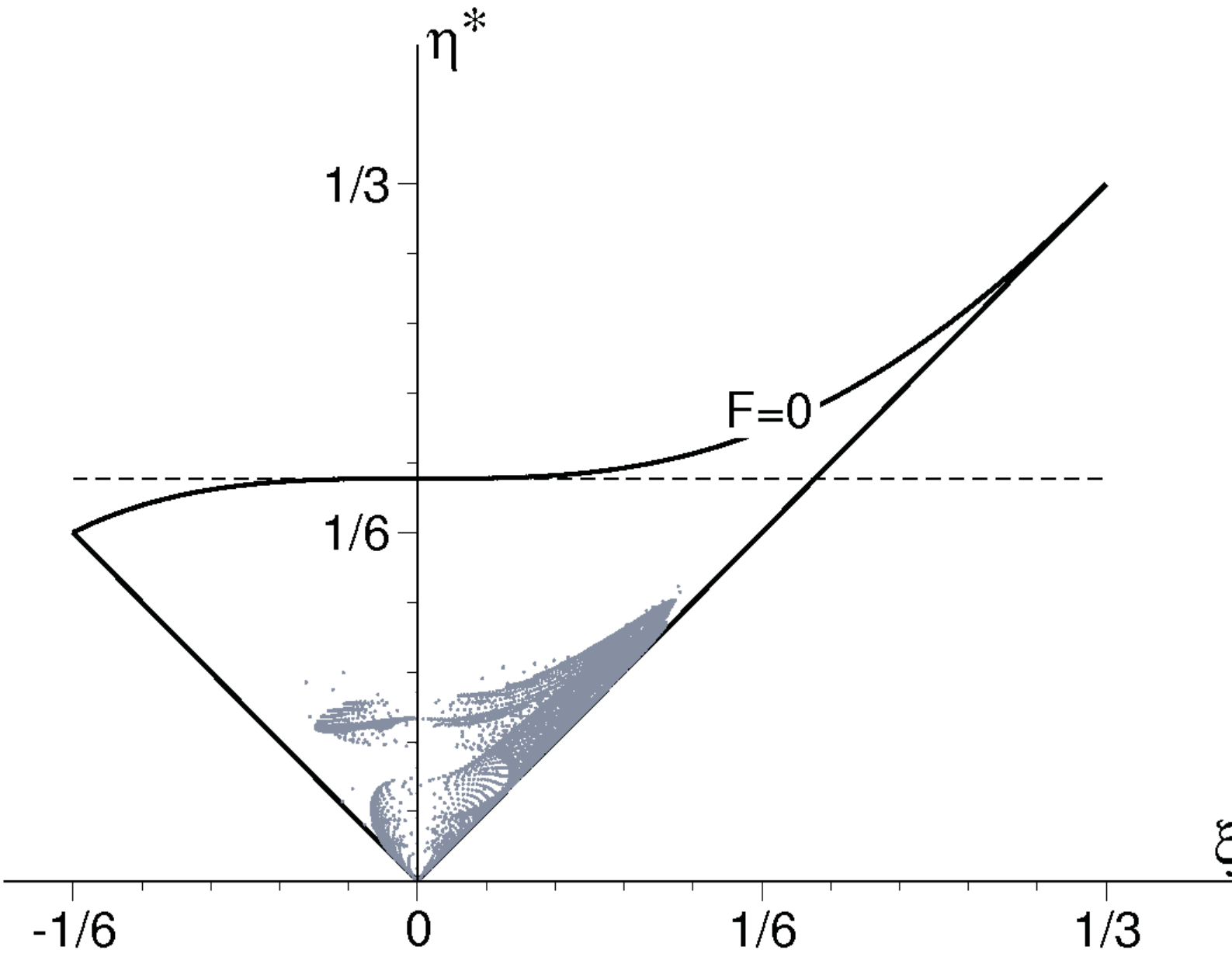

Figure 3a

Click here to download line figure: HM1_F-2.eps

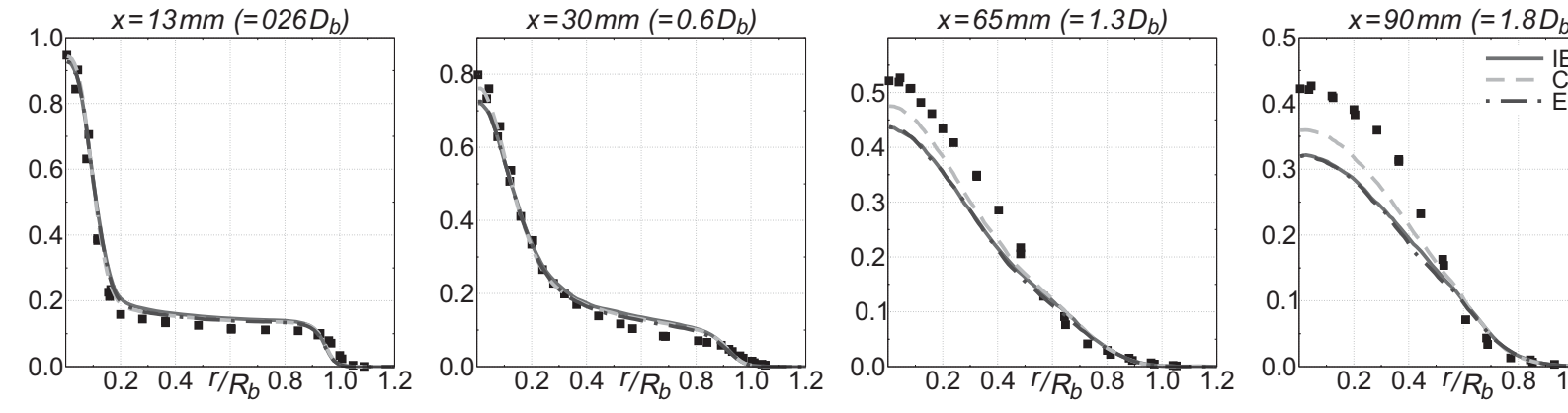

Figure 3b

Click here to download line figure: HM1_G-2.eps

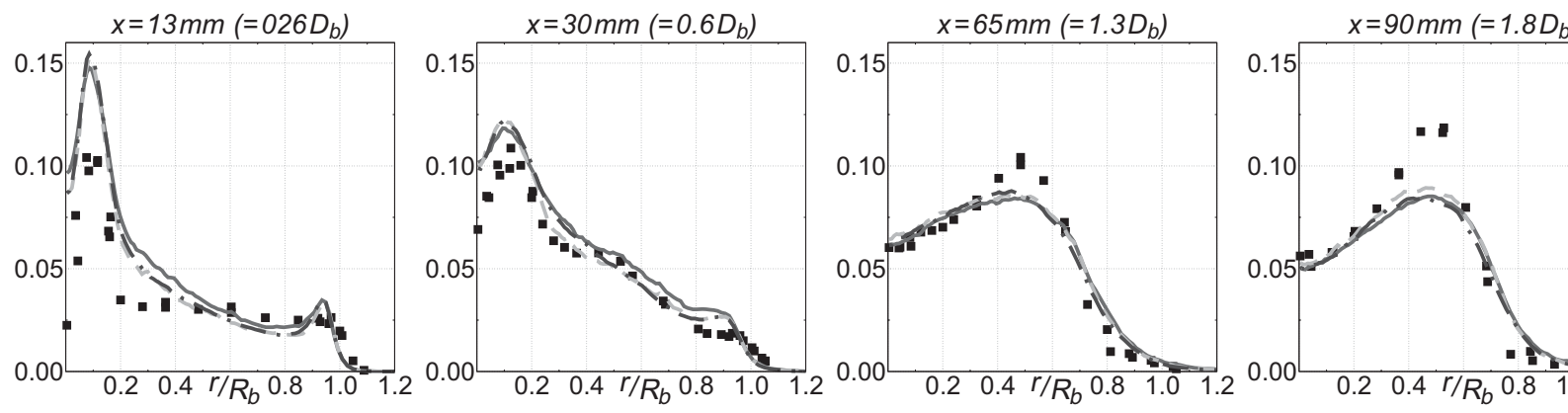

Figure 4

Click here to download line figure: HM1_C0.eps

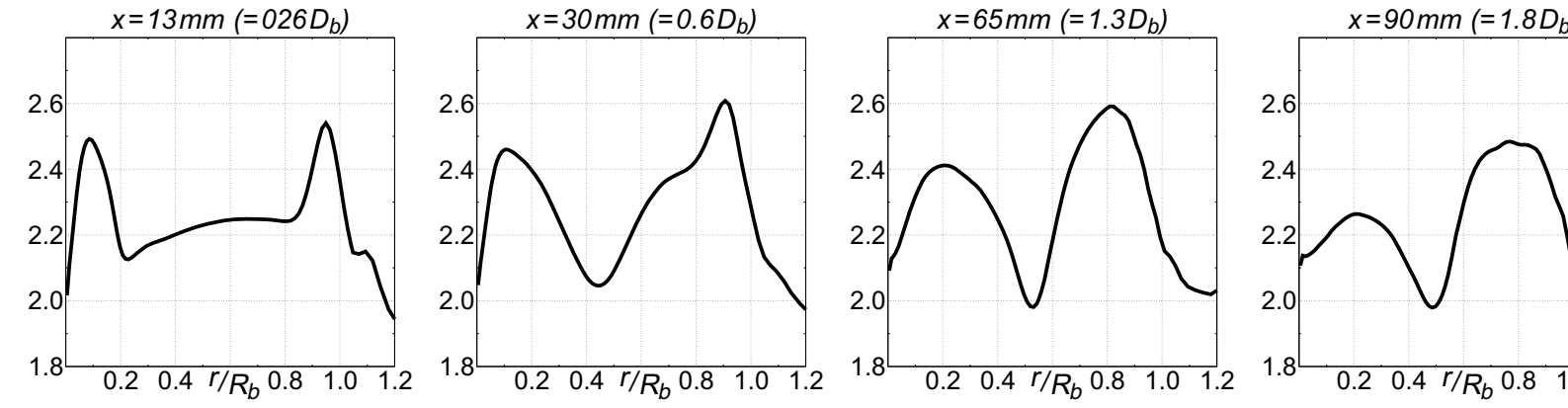

Figure 5a

Click here to download line figure: HM1_F.eps

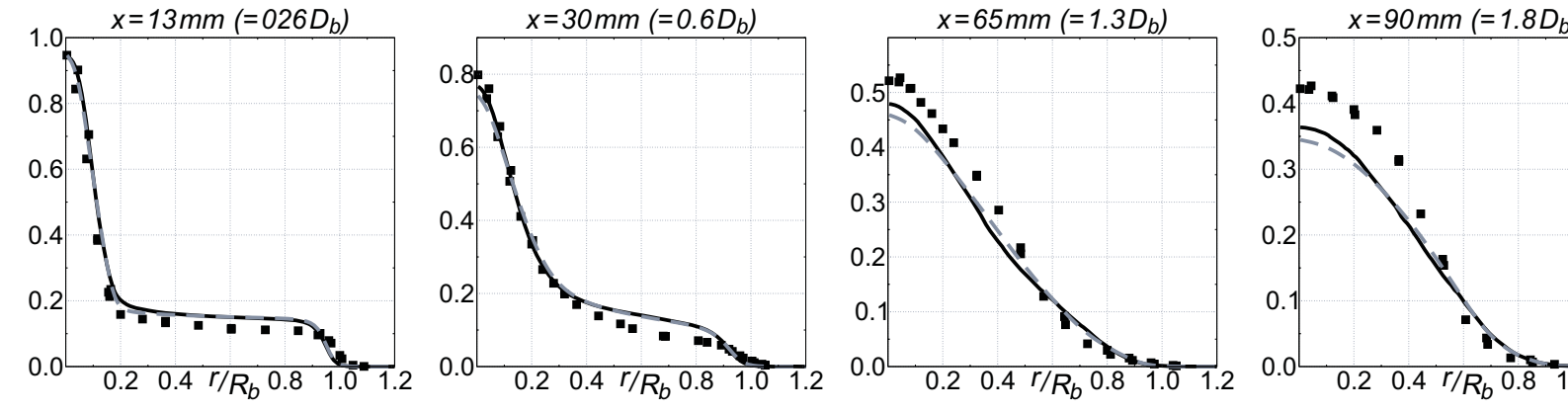

Figure 5b

Click here to download line figure: HM1_G.eps

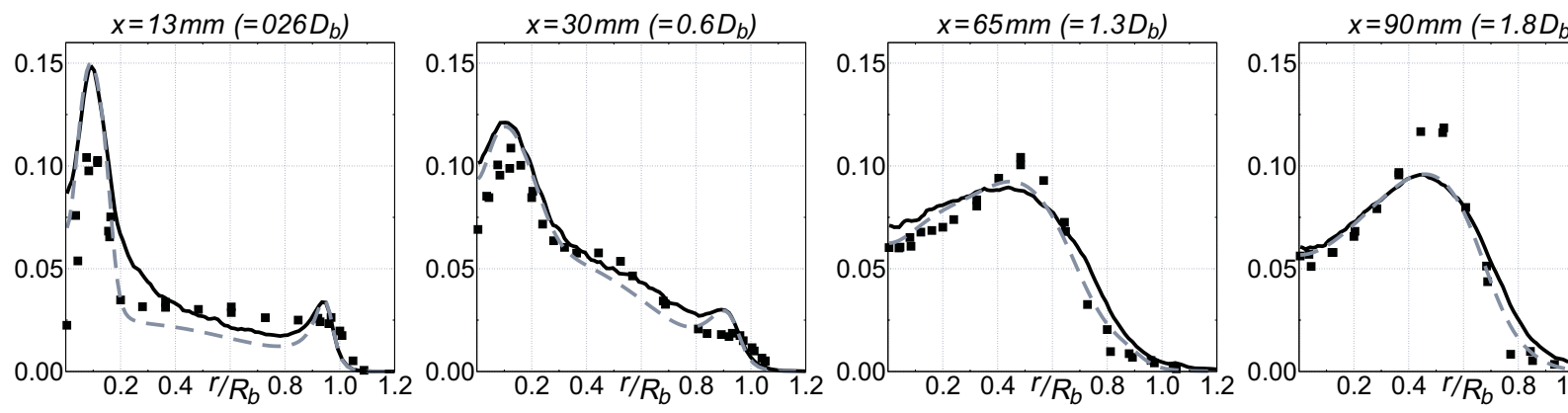

Figure 6

Click here to download line figure: HM1_comp.eps